
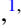






Enhanced CO tolerance of Pt clusters supported on graphene with lattice vacanciesYuji Hamamoto ^{1,2,*}, Sasfan Arman Wella ^{1,3}, Kouji Inagaki ^{1,2}, Frank Abild-Pedersen ⁴, Thomas Bligaard,⁵
Ikutaro Hamada ^{1,2} and Yoshitada Morikawa ^{1,2,6}¹*Department of Precision Engineering, Graduate School of Engineering, Osaka University, Suita, Osaka 565-0871, Japan*²*Elements Strategy Initiative for Catalysts and Batteries (ESICB), Kyoto University, Goryo-Ohara, Nishikyo-ku, Kyoto 615-8245, Japan*³*Department of Physics, Faculty of Mathematics and Natural Sciences, Institut Teknologi Bandung, Bandung 40132, Indonesia*⁴*SUNCAT Center for Interface Science and Catalysis, SLAC National Accelerator Laboratory, 2575 Sand Hill Road, Menlo Park, California 94025, USA*⁵*Catalysis Theory Center, Department of Energy Conversion and Storage, Technical University of Denmark, DK-2800 Kongens Lyngby, Denmark*⁶*Research Center for Ultra-Precision Science and Technology, Graduate School of Engineering, Osaka University, Suita, Osaka 565-0871, Japan*

(Received 18 March 2020; revised 10 June 2020; accepted 24 June 2020; published 4 August 2020)

The adsorption of CO on Pt₄ clusters supported on graphene with lattice vacancies is studied theoretically using the first-principles calculation. Our results show that the electronic structure of the graphene-supported Pt₄ clusters is significantly modified by the interaction with carbon dangling bonds. As a result the adsorption energy of CO at a Pt site decreases almost linearly with the lowering of the Pt *d*-band center, in analogy with the linear law previously reported for CO adsorption on various Pt surfaces. An exceptional behavior is found for Pt₄ supported on graphene with a tetravacancy, where CO adsorption is noticeably weaker than predicted by the shift in the *d*-band center. Detailed electronic structure analyses reveal that the deviation from the linear scaling can be attributed to lack of Pt *d* states near the Fermi level that hybridize with CO molecular orbitals. The weakening of CO adsorption on the Pt₄ clusters is considered as a manifestation of the support effect of graphene, and leads to the enhancement of CO poisoning tolerance that is crucial for developing high-performance Pt cluster catalysts.

DOI: [10.1103/PhysRevB.102.075408](https://doi.org/10.1103/PhysRevB.102.075408)**I. INTRODUCTION**

The extraordinary electronic and structural properties of graphene hold considerable potential for a wide variety of industrial applications. Among them, one of the most promising candidates is the application of graphene as a support material for metal nanoparticle catalysts. While platinum (Pt) supported on carbon (C) materials has been regarded as the most practical electrocatalyst for polymer electrolyte membrane fuel cells, the position of conventional carbon support materials is now challenged by graphene, since its large specific surface area, high chemical and electrochemical stability, and high carrier mobility are well suited for a catalyst support. A great number of experiments have been carried out in the last decade (see reviews [1–11] and references therein) and it has been demonstrated that Pt supported on graphene exhibits improved catalytic activity [12], durability [13], and carbon monoxide (CO) tolerance [12] as compared with on carbon black. In particular, high-angle annular dark-field scanning transmission electron microscopy (HAADF-STEM) has revealed the existence of extraordinarily small Pt clusters on

graphene, suggesting a possible contribution of these clusters to the high catalytic performance [12,14]. In addition, more recent HAADF-STEM measurements have even observed single Pt atoms dispersed on undoped [15,16] and nitrogen-doped [17] graphene, which show high catalytic activities and CO tolerance. Theoretically, on the other hand, first-principles calculations based on density functional theory (DFT) have been performed extensively to clarify the properties of graphene-supported Pt clusters from viewpoints of geometric [18–34] and magnetic [35–44] structures, molecular adsorptions [45–50], CO tolerance [51–54], and catalytic reactions such as CO oxidation [55–60], decomposition of O₃ [61] and methanol [62], and reduction of O₂ [63–65] and CO₂ [66]. However, the fundamental mechanism of the support effect of graphene has yet to be clarified.

In this work, we shed light on the physical aspects of the support effect of graphene on Pt clusters, with a special emphasis on CO adsorption. We perform DFT calculations of a Pt₄ cluster supported on graphene with a lattice vacancy, in which the interaction with C dangling bonds is expected to exert a significant impact on the electronic structure of Pt₄. Our results show that the center of the *d* band is lowered dramatically for Pt atoms near the vacancy, on which CO adsorption is weakened. Intriguingly, the CO adsorption energy decreases almost linearly with the lowering of the *d*-band center, indicating that the linear law previously reported for various Pt surfaces [67] is also applicable to graphene-supported Pt clusters. However, the CO adsorption energy on Pt₄ supported on graphene with a tetravacancy turns

*hamamoto@prec.eng.osaka-u.ac.jp

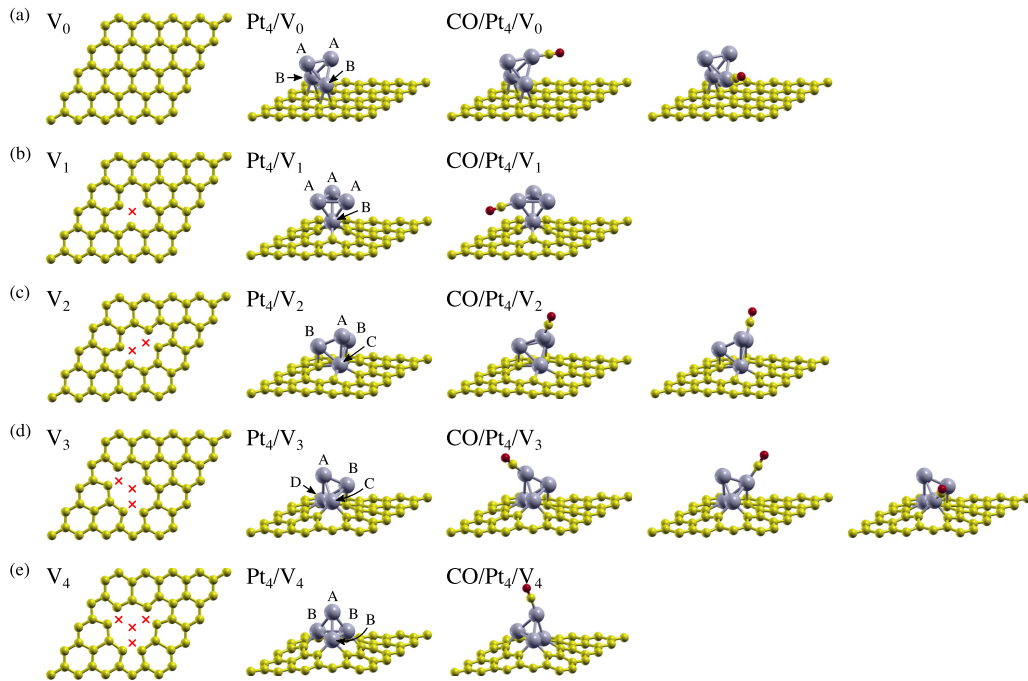


FIG. 1. Schematic views of graphene sheets without (a) and with carbon vacancies (b)–(e), and the corresponding graphene-supported Pt_4 clusters and CO adsorption structures. In the first column, crosses (\times) stand for the positions of the carbon vacancies. In the second column, inequivalent Pt atoms in each Pt_4/V_n are indicated by different labels.

out to be exceptionally small relative to the corresponding d -band center, suggesting that the d -band center alone is not sufficient to describe the whole trend of CO adsorption on graphene-supported Pt clusters. To address the problem, we propose overlap population (OP) as a more useful descriptor, on which the CO adsorption energy displays a roughly linear dependence, including the system with a tetravacancy. We also derive the perturbation formula for OP, which reveals a close relation between OP and the CO adsorption energy as described below.

II. METHODS

The DFT calculations in the present paper are carried out using the STATE [34,68] code with norm-conserving pseudopotentials [69]. The plane-wave basis set is used to expand wave functions (charge density) with cutoff energy of 64 Ry (400 Ry). Pristine graphene is modeled with a periodically repeated 5×5 unit cell of freestanding graphene with the lattice constant of 2.46 Å, and $6 \times 6 \times 1$ k points are sampled in the Brillouin zone (BZ). A lattice vacancy is formed by removing n C atoms with $n = 1, 2, 3, 4$ from the pristine graphene, and a supported Pt nanoparticle is modeled with a tetrahedral cluster composed of four Pt atoms (Pt_4). The finite-size effect in the system with $n = 4$ is examined by using a 10×10 unit cell, for which $3 \times 3 \times 1$ k points are sampled in the BZ. As a probe of the support effect, a CO molecule is adsorbed on the graphene-supported Pt_4 cluster. The exchange-correlation energy and potential are described within the generalized gradient approximation using the Perdew-Burke-Ernzerhof (PBE) [70] functional, which has been widely adopted in previous calculations of Pt clusters on graphene [51,52,55–60]. The structure of each system is

relaxed until the atomic forces fall below 8.24×10^{-2} nN (5.14×10^{-2} eV/Å). Spin polarization is taken into account for a free Pt_4 cluster and graphene with an odd-numbered vacancy, while the other systems are assumed to be spin unpolarized. A vacuum layer of 30 Å is introduced and the effective screening medium method [71,72] is used to eliminate the spurious electrostatic interaction with the periodic images.

III. RESULTS AND DISCUSSION

A. Pt_4 clusters supported on graphene with lattice vacancies

The relaxed structures of graphene with lattice vacancies are depicted in the first column of Fig. 1, where V_n stands for graphene with n C vacancies with $n = 0, 1, \dots, 4$. Around the lattice vacancies, the honeycomb lattice is reconstructed to saturate dangling bonds by forming nonhexagonal rings. For example, Jahn-Teller distortion breaks D_{3h} symmetry of a monovacancy in V_1 [73,74]. The formation energy of V_n is defined as

$$E_{\text{form}}(\text{V}_n) = E(\text{V}_n) - E(\text{V}_0) + n\mu_{\text{C}}, \quad (1)$$

where $E(\text{V}_n)$ denotes the total energy of V_n , and μ_{C} is the C chemical potential defined as the total energy of pristine graphene V_0 per C atom. The formation energies for V_1 , V_2 , V_3 , and V_4 are calculated to be 7.77, 8.10, 11.31, and 12.17 eV, respectively, which compare well with previous calculations; see Refs. [75–77] and references therein. The value of $E_{\text{form}}(\text{V}_1)$ is also in agreement with the experimental results of >6.6 eV estimated from vacancy concentration in quenched graphite [78] and 7.3 ± 1 eV from lattice parameter change in irradiated graphite [79].

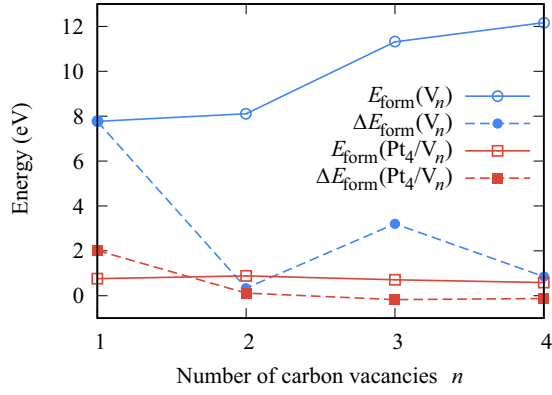


FIG. 2. Formation energies of graphene sheets with a lattice vacancy V_n (o) and graphene-supported Pt_4 clusters Pt_4/V_n (□). Filled circles (●) and squares (■) correspond to the energy differences defined by Eqs. (3) and (8), respectively.

The formation energies of large vacancies can be reduced by removing C atoms one by one, whose energy cost is given by the difference

$$\begin{aligned} \Delta E_{\text{form}}(V_n) &= E_{\text{form}}(V_n) - E_{\text{form}}(V_{n-1}) \\ &= E(V_n) - E(V_{n-1}) + \mu_C. \end{aligned} \quad (2)$$

We plot $E_{\text{form}}(V_n)$ and $\Delta E_{\text{form}}(V_n)$ as a function of the number of C vacancies in Fig. 2, where odd-numbered vacancies still give larger $\Delta E_{\text{form}}(V_n)$ than even-numbered ones. This is because the formation of an odd-numbered vacancy is accompanied by at least one unsaturated dangling bond [75], which results in spin polarization of odd-numbered vacancies [80].

We next consider adsorption of a Pt_4 cluster on top of each vacancy and calculate the adsorption energy

$$E_{\text{ads}}(\text{Pt}_4/V_n) = E(\text{Pt}_4/V_n) - E(\text{Pt}_4) - E(V_n), \quad (4)$$

where $E(\text{Pt}_4/V_n)$ and $E(\text{Pt}_4)$ denote the total energies of the adsorbed system Pt_4/V_n and a free Pt_4 cluster, respectively. By comparing the adsorption energies for several structures, we determine the most stable adsorption structure of Pt_4 on each vacancy as shown in the second column of Fig. 1. On pristine graphene, a three-legged adsorption structure is in fact slightly more stable than the two-legged one shown in Fig. 1(a), with $E_{\text{ads}}(\text{Pt}_4/V_0) = -1.27$ and -1.25 eV, respectively. However, the former is destabilized upon adsorption of a CO molecule, and thus we here adopt the latter as the adsorption structure for Pt_4/V_0 . In contrast to the weak adsorption on V_0 , Pt_4 adsorbs more strongly on graphene with the vacancies; i.e., the Pt_4 adsorption energies on V_1 , V_2 , V_3 , and V_4 are calculated to be -7.00 , -7.23 , -10.60 , and -11.58 eV, respectively. Note that the Pt_4 adsorption energies tend to balance the large energy costs for the formation of the vacancies. Namely, if we assume that V_n is formed along with the adsorption of Pt_4 , the formation energy of Pt_4/V_n defined as

$$\begin{aligned} E_{\text{form}}(\text{Pt}_4/V_n) &= E_{\text{form}}(V_n) + E_{\text{ads}}(\text{Pt}_4/V_n) \\ &= E(\text{Pt}_4/V_n) - E(\text{Pt}_4) - E(V_0) + n\mu_C \end{aligned} \quad (5)$$

is much smaller than $E_{\text{form}}(V_n)$ as shown in Fig. 2, although the formation of Pt_4/V_n is still endothermic. In analogy with

Eq. (3), we also consider the difference

$$\begin{aligned} \Delta E_{\text{form}}(\text{Pt}_4/V_n) &= E_{\text{form}}(\text{Pt}_4/V_n) - E_{\text{form}}(\text{Pt}_4/V_{n-1}) \\ &= E(\text{Pt}_4/V_n) - E(\text{Pt}_4/V_{n-1}) + \mu_C, \end{aligned} \quad (7)$$

which describes the energy cost to form Pt_4/V_n by removing a C atom from Pt_4/V_{n-1} . Although it costs large energy of 2 eV to remove the first C atom, $\Delta E_{\text{form}}(\text{Pt}_4/V_n)$ becomes even negative, i.e., -0.17 and -0.12 eV for $n = 3$ and 4, respectively, as shown in Fig. 2. This reveals that Pt_4 adsorbed on graphene acts as a catalyst that facilitates the expansion of lattice vacancies, justifying our models of Pt clusters supported on large vacancies. This is qualitatively consistent with the results of TEM measurements, in which Pt atoms catalyze the dissociation of C–C bonds at graphene edges [81,82]. Note that, by definition, $\Delta E_{\text{form}}(\text{Pt}_4/V_1)$ is larger than $E_{\text{form}}(\text{Pt}_4/V_1)$ by $E_{\text{ads}}(\text{Pt}_4/V_0)$, and thus forming V_1 along with the adsorption of Pt_4 is a more possible scenario for the formation of Pt_4/V_1 .

B. Local density of states projected onto the Pt d states

To investigate the support effect of graphene on the electronic structure of Pt_4 , we first examine the local density of states (LDOS) projected onto the d states of each Pt atom in Pt_4/V_n . The calculated LDOS (ρ_d) is plotted as a function of energy ε measured from the Fermi level ε_F in Fig. 3, where, e.g., Pt_A/V_n in each panel stands for the Pt atom(s) labeled as A on V_n in the second column of Fig. 1. Special care should be taken for treating ε_F , since it is ill defined for the DFT calculations of gapped systems. In Fig. 3 (and Fig. 5 seen below), we determine ε_F using the method as illustrated in Appendix A.

The LDOSs reflect the interactions between the Pt d states and graphene, and their trend can be captured by introducing the d -band center defined as

$$\varepsilon_d = \frac{\int \varepsilon \rho_d(\varepsilon) d\varepsilon}{\int \rho_d(\varepsilon) d\varepsilon}, \quad (9)$$

where the energy integral is taken from -15 eV to 4 eV with respect to ε_F . The calculated d -band centers are indicated by the vertical lines in Fig. 3, and the detailed values are summarized in Table I. From Fig. 3(a), one can see that Pt_A/V_0 and Pt_B/V_0 have little difference in ρ_d , but the latter shows high peaks at slightly lower energies than the former. As a result the d -band centers of Pt_A/V_0 and Pt_B/V_0 are calculated to be -1.64 and -2.39 eV, respectively. On the other hand, Pt_A/V_1 and Pt_B/V_1 exhibit significant difference in LDOS; i.e., the peak structures are retained for the former, while the d band of the latter is broadened dramatically as shown in Fig. 3(b). The difference is due to the strong interaction between Pt_B and three dangling bonds of the monovacancy, which is also reflected in the d -band centers of -1.65 and -4.15 eV for Pt_A/V_1 and Pt_B/V_1 , respectively. A similar difference is found between Pt_A/V_2 and Pt_C/V_2 , whose d -band centers are -1.82 and -4.25 eV, respectively. The even deeper d -band center of the latter reflects the broader d band due to the interaction between Pt_C and four dangling bonds of the divacancy. Apparently, Pt_B/V_2 also interacts with a dangling bond, but its narrower d band with $\varepsilon_d = -2.33$ eV suggests that the d states of Pt_B/V_2 are rather close to those of Pt_A/V_2 .

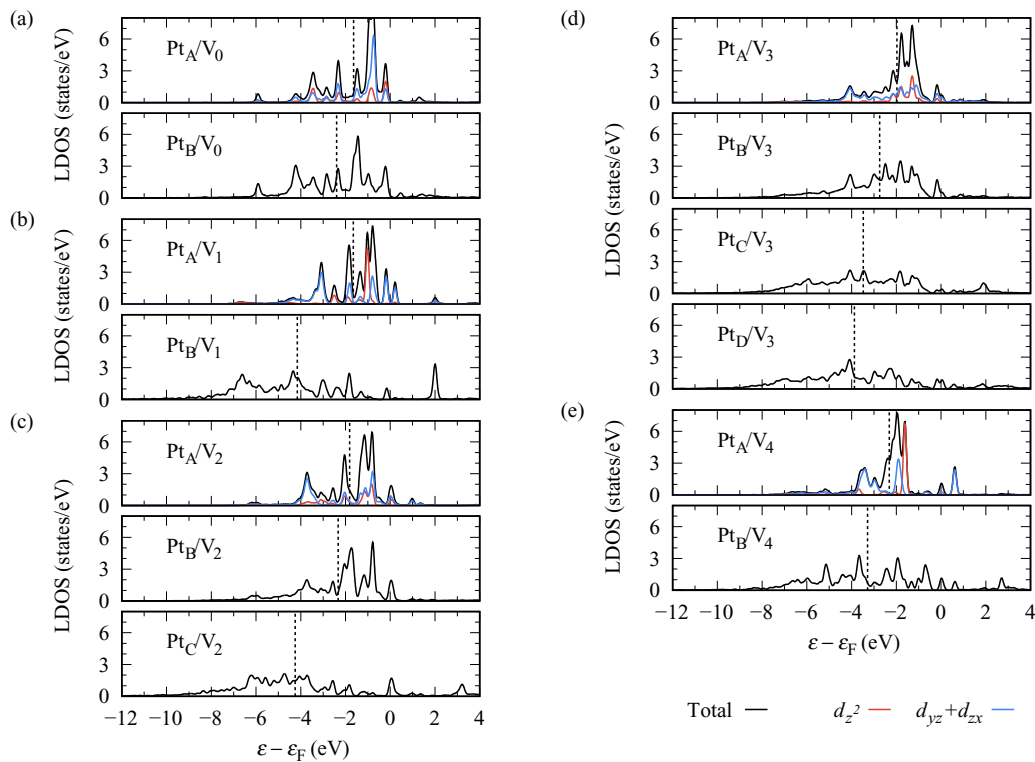


FIG. 3. LDOS projected onto the Pt d states plotted as a function of energy measured from the Fermi level. The peaks are smeared by a Gaussian of width 0.1 eV. The results for Pt_4/V_n with $n = 0, 1, \dots, 4$ are shown in panels (a)–(e), respectively. In each panel, the d -band centers are indicated by vertical lines. The LDOSs projected onto $\text{Pt}_{d_{z^2}}$ and $(d_{yz} + d_{zx})$ states are also shown in the results for Pt_A/V_n , where the z axis is perpendicular to the face of Pt_4 opposite to Pt_A .

The site dependence of the LDOS can be observed more clearly for Pt_4/V_3 , since the highly asymmetric adsorption structure makes the four Pt atoms inequivalent [see Fig. 1(d)]. Namely, the d -band center is shifted downward monotonically as -1.97 , -2.75 , -3.48 , and -3.87 eV for Pt_A/V_3 , Pt_B/V_3 , Pt_C/V_3 , and Pt_D/V_3 , respectively, as shown in Fig. 3(d). Pt_C/V_3 and Pt_D/V_3 are analogous to Pt_B/V_4 in that they interact with two dangling bonds of a vacancy. As a result, $\varepsilon_d = -3.29$ eV for Pt_B/V_4 is close to the d -band centers of Pt_C/V_3 and Pt_D/V_3 . From the comparison among the four graphene-supported Pt_4 clusters, one can also find that the d -band center of the topmost Pt atom is lowered monotonically with the size of the lattice vacancy. In particular, Pt_A/V_4 exhibits a relatively deep d -band center of -2.31 eV, despite the fact that the Pt atom has no direct bond to the tetravacancy.

C. CO adsorption on the graphene-supported Pt_4 clusters

We next investigate the support effect of graphene on molecular adsorption. We here take CO as an example, which is one of the most important adsorbates relevant to fuel cell catalysts. We examine several adsorption structures of CO on Pt_4/V_n and calculate the CO adsorption energy defined as

$$E_{\text{ads}}(\text{CO}/\text{Pt}_4/\text{V}_n) = E(\text{CO}/\text{Pt}_4/\text{V}_n) - E(\text{CO}) - E(\text{Pt}_4/\text{V}_n), \quad (10)$$

where $E(\text{CO}/\text{Pt}_4/\text{V}_n)$ and $E(\text{CO})$ denote the total energies of the adsorption system $\text{CO}/\text{Pt}_4/\text{V}_n$ and a free CO molecule, respectively. Among a wide variety of CO adsorption structures,

we here focus on the adsorption at on-top sites of Pt_4/V_n , since CO adsorbs less strongly at bridge and hollow sites of a free Pt_4 cluster. The calculated adsorption energies and relevant bond lengths are summarized in Table I. Comparison of the adsorption energies reveals that CO prefers to adsorb at the topmost site, i.e., Pt_A as depicted in the third column of Fig. 1, while CO gets destabilized as the adsorption site gets closer to graphene, and the adsorption at the bottommost Pt atoms turns out to be unstable except for Pt_4/V_0 . The site dependence of the CO adsorption energy is closely related to the geometry of the adsorption system as shown in Figs. 4(a) and 4(b), where the adsorption energy is plotted as functions of Pt–C and C–O bond lengths, respectively, with C being the C atom in CO. Figure 4(a) clearly indicates that $E_{\text{ads}}(\text{CO}/\text{Pt}_4/\text{V}_n)$ increases monotonically as the Pt–C bond is shortened, in agreement with the tendency that CO closer to Pt_4/V_n has larger overlap between CO molecular orbitals (MOs) and Pt d states. In contrast, Fig. 4(b) displays a monotonic increase in $E_{\text{ads}}(\text{CO}/\text{Pt}_4/\text{V}_n)$ with the elongation of the C–O bond, suggesting that the back-donation from Pt d states to the antibonding CO 2π orbital contributes to the CO adsorption on Pt_4/V_n . Note, however, that the contribution of the donation from the CO 5σ orbital to Pt d states cannot be inferred from Fig. 4(b), since CO 5σ is predominantly localized at the C atom.

In Fig. 4(c), we also plot $E_{\text{ads}}(\text{CO}/\text{Pt}_4/\text{V}_n)$ as a function of ε_d in the spirit of the d -band model [83–85], where the nature of the d states of a metal surface is represented by ε_d . Intriguingly, $E_{\text{ads}}(\text{CO}/\text{Pt}_4/\text{V}_n)$ displays an almost linear

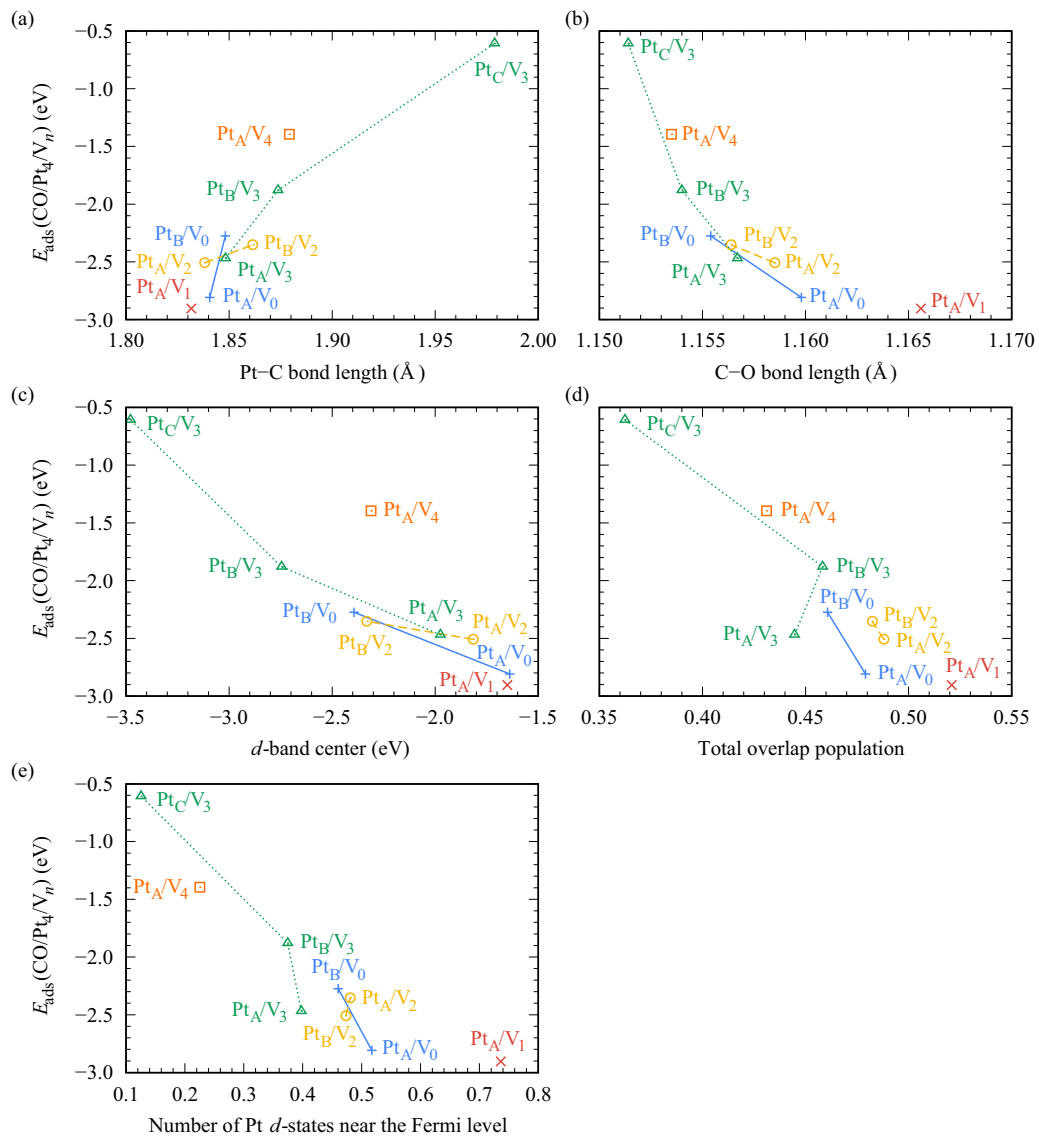


FIG. 4. CO adsorption energy plotted as a function of the Pt-C bond length (a), the C-O bond length (b), the d -band center (c), the total overlap population (d), and the number of Pt d states near the Fermi level (e). In each panel, pluses (+), crosses (\times), circles (\circ), triangles (Δ), and squares (\square) correspond to the results for Pt_A/V_n with $n = 0, 1, \dots, 4$, respectively. Solid, dashed, and dotted lines are drawn to guide the eye. In panel (e), the number of Pt d states near ε_F is estimated by integrating the LDOS in Fig. 3 from -0.25 eV to 0.25 eV with respect to ε_F .

relation with ε_d , in analogy with CO adsorbed on various Pt surfaces [67]. An exception is CO adsorbed at Pt_A/V_4 , whose adsorption energy deviates significantly from the linear law. It is tempting to think that the deviation is attributed to the fact that the tetravacancy is too large relative to the unit cell or that the structure of Pt_4/V_4 is distorted significantly upon the adsorption of CO. However, $E_{\text{ads}}(\text{CO}/\text{Pt}_4/\text{V}_4)$ remains almost unchanged even though the 10×10 unit cell is adopted, and is decreased to -1.12 eV if the geometry of Pt_4/V_4 is fixed during CO adsorption, the latter of which suggests that CO adsorption is in fact stabilized by the distortion of Pt_4/V_4 . The deviation from the linear law indicates that the d -band center alone is not sufficient to explain the mechanism of CO adsorption on Pt_4/V_n . It should be noted that $E_{\text{ads}}(\text{CO}/\text{Pt}_4/\text{V}_4)$ is even smaller than the CO adsorption energy of -1.70 eV at the on-top site of the Pt(111) surface at $1/9$ coverage. This

is particularly important from an applicational point of view, since the tolerance for CO poisoning is crucial for developing high-performance metal catalysts. Our results demonstrate that the interaction with large vacancies in graphene can enhance the CO tolerance of supported Pt clusters, which has indeed been suggested experimentally as an origin of the high catalytic activity of graphene-supported Pt clusters [12,14]. Note that the graphene supports used in these experiments are expected to have lattice vacancies introduced in the preparation process of reducing graphene oxide.

D. Overlap population analysis

To gain more insight into the role of CO MOs in CO adsorption on Pt_4/V_n , we finally investigate the density of states weighted by OP [86–88], often referred to as crystal

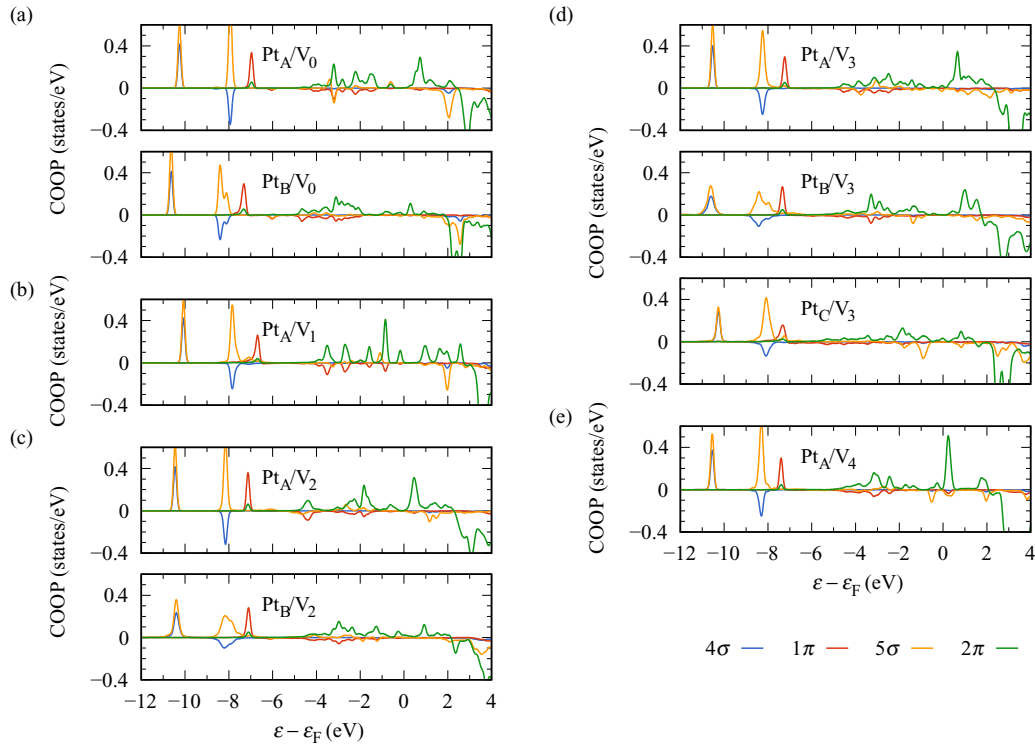


FIG. 5. COOP plotted as a function of energy measured from the Fermi level. The peaks are smeared by a Gaussian of width 0.1 eV. The results for Pt_4/V_n with $n = 0, 1, \dots, 4$ are shown in panels (a)–(e), respectively. In each panel, the COOP curves for CO 4σ (blue), 1π (red), 5σ (orange), and 2π (green) are shown.

orbital overlap population (COOP) [89,90]. The calculated COOP curves between CO MOs and all the states of Pt_4/V_n are shown in Fig. 5, where positive (negative) peaks represent bonding (antibonding) states formed as a result of CO adsorption. The behavior of the COOP peaks can easily be understood from the perturbative expression for the OP-weighted density of states, i.e., Eq. (B30) in Appendix B. Among the four CO MOs considered here, low-lying 4σ and 1π have both positive and negative peaks below ε_F in the COOP curves, which indicates that the bonding and antibonding contributions of these MOs almost cancel each other out. On the other hand, the existence of negative (positive) peaks derived from 5σ (2π) above (below) ε_F suggests that this MO contributes attractively to the CO adsorption through the donation (back-donation) processes. The latter behavior is consistent with the Blyholder model of CO adsorption on Pt surfaces [91].

The contributions of these MOs can be compared quantitatively by calculating OP per MO, which is obtained from the integral of COOP below ε_F . The calculated results for OP are summarized in Table I, which shows that 5σ contributes slightly more than 2π except for Pt_C/V_3 , while the contributions from 4σ and 1π orbitals are negligibly small. More importantly, the results for 5σ exhibit a characteristic dependence on the CO adsorption site. Namely, adsorption sites farther away from graphene tend to give larger OPs except for Pt_A/V_3 . In addition, OP for 5σ is largest at Pt_A/V_1 , while it is relatively small at Pt_A/V_4 as compared with other topmost Pt atoms. These behaviors are quite similar to the site depen-

dence of $E_{\text{ads}}(\text{CO}/\text{Pt}_4/\text{V}_n)$ discussed in the previous section. On the other hand, the relation with $E_{\text{ads}}(\text{CO}/\text{Pt}_4/\text{V}_n)$ is less clear for 2π , unlike the dependence of $E_{\text{ads}}(\text{CO}/\text{Pt}_4/\text{V}_n)$ on the C–O bond length shown in Fig. 4(b), where the elongation of the C–O bond indicates the hybridization of 2π . Still, the OPs of 5σ and 2π tend to decrease with the size of the vacancy. In the last column of Table I, we also show the total OP for each CO adsorption structure, which retains the similarity to the CO adsorption energy. Indeed, the CO adsorption energy as a function of the total OP exhibits roughly linear dependence including $\text{CO}/\text{Pt}_4/\text{V}_4$ as shown in Fig. 4(d), indicating that the CO adsorption energy is sensitive to the apparently small difference in the total OP.

The relation between the CO adsorption energy and the total OP can be understood from the fact that the hybridization between CO MOs and Pt d states is mainly responsible for the CO adsorption on Pt_4/V_n . We consider the interaction between two states k and l with unperturbed energies ε_k and ε_l , respectively. To the second order in the interactions, OP between k and l is approximated as

$$p_{kl} = \frac{2\text{Re}[S_{kl}V_{lk}]}{\varepsilon_k - \varepsilon_l}, \quad (11)$$

where $\varepsilon_k < \varepsilon_F < \varepsilon_l$, and S_{kl} (V_{lk}) denotes the overlap integral (coupling matrix element) between k and l . See Appendix B for the derivation of Eq. (11). Specifically, k and l correspond to an occupied state of CO (Pt_4/V_n) and an unoccupied state of Pt_4/V_n (CO), respectively, for a donation (back-donation) process. In the Mulliken-Wolfsberg-Helmholz (MWH)

TABLE I. d -band center and CO adsorption energy in eV for each Pt site, lengths of Pt-C and C-O bonds in Å, where C denotes the C atom bound to the O atom in CO, and the overlap population between the CO molecular orbitals and the states of Pt_4/V_n . In the column of C-O bond length, the value in the parentheses shows the relative difference from a free CO molecule, whose bond length is calculated to be 1.133 Å.

Site	E_d (eV)	$E_{\text{ads}}(\text{CO}/Pt_4/V_n)$ (eV)	Bond length (Å)		Overlap population				Total
			Pt-C	C-O	4σ	1π	5σ	2π	
Pt_A/V_0	-1.64	-2.81	1.841	1.160 (+2.3%)	0.01	-0.02	0.27	0.22	0.48
Pt_B/V_0	-2.39	-2.27	1.848	1.155 (+2.0%)	0.00	-0.03	0.26	0.23	0.46
Pt_A/V_1	-1.65	-2.90	1.832	1.166 (+2.9%)	0.01	-0.03	0.29	0.25	0.52
Pt_B/V_1	-4.15								
Pt_A/V_2	-1.82	-2.51	1.838	1.159 (+2.2%)	0.01	-0.02	0.28	0.23	0.49
Pt_B/V_2	-2.33	-2.35	1.862	1.156 (+2.0%)	0.01	-0.02	0.27	0.24	0.48
Pt_C/V_2	-4.25								
Pt_A/V_3	-1.97	-2.47	1.848	1.157 (+2.1%)	0.00	-0.02	0.25	0.21	0.44
Pt_B/V_3	-2.75	-1.88	1.874	1.154 (+1.8%)	0.00	-0.02	0.25	0.22	0.46
Pt_C/V_3	-3.48	-0.61	1.979	1.151 (+1.6%)	0.00	-0.02	0.18	0.20	0.36
Pt_D/V_3	-3.87								
Pt_A/V_4	-2.31	-1.40	1.879	1.154 (+1.8%)	0.00	-0.02	0.25	0.20	0.43
Pt_B/V_4	-3.29								

approximation $V_{lk} \simeq -\alpha S_{lk}$ with $\alpha > 0$ [92,93], p_{kl} is proportional to the first term of the energy correction to state k given by

$$\Delta \varepsilon_{kl} = \frac{|V_{kl}|^2}{\varepsilon_k - \varepsilon_l} - S_{kl} V_{lk}, \quad (12)$$

where the second term describes the energy cost for orthogonalization. $E_{\text{ads}}(\text{CO}/Pt_4/V_n)$ is roughly given by the sum of $\Delta \varepsilon_{kl}$ over k and l , which correspond to an occupied (unoccupied) orbital of CO and an unoccupied (occupied) state of Pt_4/V_n , respectively, in a donation (back-donation) process. Thus, $E_{\text{ads}}(\text{CO}/Pt_4/V_n)$ is expected to scale linearly with the total OP as seen in Fig. 4(d).

To clarify the origin of the decrease in OP with the size of the vacancy, we also plot the LDOSs projected onto the d_{z^2} and $(d_{yz} + d_{zx})$ states of Pt_A/V_n in Fig. 3. In each system, we take the z axis perpendicularly to the face of Pt_4 opposite to Pt_A so that 5σ (2π) has largest overlap with d_{z^2} ($d_{yz} + d_{zx}$) when the CO axis is parallel to the z direction. However, the adsorbed CO is in general inclined from the z axis as can be seen from the third column of Fig. 1, suggesting that d_{z^2} peaks distributed below ε_F interact repulsively with 5σ . Alternatively, the inclined adsorption structure enables 5σ (2π) to overlap with $d_{yz} + d_{zx}$ (d_{z^2}), and thus the bond between CO and Pt_A/V_n consists of several interactions between CO MOs and Pt d states. In the LDOS of Pt_A/V_0 , for example, the peak just below ε_F is composed of d_{z^2} and $d_{yz} + d_{zx}$, both of which hybridize with 5σ and 2π . On the other hand, Pt_A/V_1 shows two peaks derived from $d_{yz} + d_{zx}$ near ε_F , while a large d_{z^2} peak appears at -1 eV, which indicates that the former predominantly hybridize with 5σ and 2π . For Pt_A/V_2 and Pt_A/V_3 , the peak near ε_F , which is composed of d_{z^2} and $d_{yz} + d_{zx}$, is smaller than those for Pt_A/V_0 and Pt_A/V_1 , in agreement with the decreases in OP. Pt_A/V_4 also shows a peak near ε_F but its $d_{yz} + d_{zx}$ component is negligibly small, while the large $d_{yz} + d_{zx}$ peaks at 0.6 and -1.9 eV scarcely

hybridize with 5σ and 2π , respectively. Moreover, the d_{z^2} states at Pt_A/V_4 are almost fully occupied, and the large d_{z^2} peak at -1.6 eV interacts repulsively with 5σ . To confirm the importance of the d states near ε_F , we also plot the CO adsorption energy as a function of the number of d states near ε_F (N_F) as shown in Fig. 4(e), where N_F is estimated by integrating the LDOS in Fig. 3 from -0.25 eV to 0.25 eV with respect to ε_F . Note that the peaks in the energy range mainly consist of d_{z^2} and/or $d_{yz} + d_{zx}$ states. Figure 4(e) shows that $E_{\text{ads}}(\text{CO}/Pt_4/V_n)$ increases roughly linearly with N_F , in analogy with the dependence on the total OP seen in Fig. 4(d). From these observations, we conclude that OP is mainly determined by the electronic structures of Pt d_{z^2} and $(d_{yz} + d_{zx})$ states, and in particular the exceptionally small CO adsorption energy at Pt_A/V_4 can be attributed to the lack of these d states near ε_F , as well as the repulsion between Pt d_{z^2} and CO 5σ .

IV. SUMMARY

We have investigated theoretically CO adsorption on Pt_4 clusters supported on graphene with lattice vacancies. The analysis of the LDOS projected onto the Pt d states has revealed that the d -band center is lowered significantly for Pt atoms near a vacancy, reflecting the interaction with C dangling bonds. As a result the adsorption energy of CO at a Pt site decreases almost linearly with the lowering of the Pt d -band center with an exception of Pt_4/V_4 , where CO adsorption is unusually weak relative to the corresponding d -band center. From a detailed analysis of OP between CO MOs and the states of Pt_4/V_n , we have also shown that the total OP tends to decrease with the size of the vacancy, and that the CO adsorption energy depends roughly linearly on the total OP and on the number of d states near ε_F , including CO adsorbed on Pt_4/V_4 . Thus, we conclude that the exceptionally weak CO adsorption on Pt_4/V_4 can be attributed to the lack

of Pt d states near ε_F that have large overlap with CO 5σ and 2π orbitals. The approach based on OP is also applicable to other adsorption systems, in particular those in which the overlap between the electronic states of the adsorbate and the surface plays an essential role in the stability of the adsorption structure. Although further theoretical analyses are required for the elucidation of the origin of the high catalytic activity of graphene-supported Pt clusters, it is highly expected that the support effect of graphene on the Pt d states not only enhances CO tolerance, but also has a significant impact on the catalytic activity.

ACKNOWLEDGMENTS

We thank Prof. Jens K. Nørskov, Junji Nakamura, and Takahiro Kondo for valuable discussions. S.A.W. acknowledges financial support by the Marubun Research Promotion Foundation. F.A-P. acknowledges support from the US Department of Energy, Office of Science, Office of Basic Energy Sciences, Chemical Sciences, Geosciences, and Biosciences Division, Catalysis Science Program, to the SUNCAT Center for Interface Science and Catalysis. The present study was partly supported by Grants-in-Aid for Scientific Research on Innovative Areas “3D Active-Site Science” (Grants No. JP26105010 and No. JP26105011), and “Elements Strategy Initiative for Catalysts & Batteries” (ESICB) of the Ministry of Education, Culture, Sports, Science, and Technology, Japan (MEXT) (Grant No. JPMXP0112101003). The numerical calculations in this work have been done with the facilities of the Supercomputer Center, Institute for Solid State Physics, University of Tokyo.

APPENDIX A: DETERMINATION OF THE FERMI LEVELS OF GAPPED SYSTEMS

In Secs. III B and III D, we have calculated the d -band center and overlap population, which depend on the reference from which energy levels are measured. Although the Fermi level ε_F is often used as the energy reference, it is well known that ε_F is ill defined for the DFT calculations of gapped systems. In the present systems, the formation of a vacancy or the interaction with a Pt cluster opens a finite gap in the otherwise gapless band structure of graphene. This hinders the comparison of the d -band center and overlap population among different systems, for which ε_F varies with the size of the energy gap. To address this problem, we have corrected the energy levels in Figs. 3 and 5 through the helium (He) $1s$ level, as illustrated in what follows.

The first step of our approach is to determine the He $1s$ level by considering a system composed of pristine graphene and a He atom in the vacuum layer. The gapless band structure of graphene remains almost unchanged as long as the He atom stays far away from graphene. This enables us to measure the He $1s$ level from ε_F , which coincides with the Dirac point of the band structure of graphene. By comparing the results for several unit cells, the He $1s$ level is determined to be -11.46 eV below ε_F . We next add a He atom to the vacuum layer of Pt_4/V_n or $\text{CO}/\text{Pt}_4/\text{V}_n$, in which the He $1s$ level obtained from the DFT calculation is in general shifted from the above value, reflecting the ambiguity in ε_F . Since the

other energy levels are shifted parallel to the He $1s$ level, the correct energy levels as well as ε_F are obtained by compensating the energy difference between the two He $1s$ levels. It is expected that the correction method presented here is also applicable to other systems with a sufficient vacuum layer.

APPENDIX B: PERTURBATION THEORY FOR ADSORPTION SYSTEMS

In Sec. III D, we have shown the perturbation formulas for the overlap population (11) and the energy correction (12) based on a nonorthogonal basis. Note that perturbation formulas are usually derived by using an orthogonal basis, since it is in general possible to form an orthogonal basis for a Hermitian Hamiltonian. However, this is not the case for the discussion of, e.g., overlap population, in which the basis for the system is assumed to consist of several orthogonal bases formed separately for respective subsystems. Here we briefly summarize the perturbation theory based on such a nonorthogonal basis, and show an application to molecular adsorption on a surface.

1. Preliminaries

Consider a system composed of several subsystems weakly interacting with each other. The Hamiltonian of the system consists of two terms as

$$H = H_0 + V, \quad (\text{B1})$$

where H_0 is the Hamiltonian of the respective subsystems and V describe the interaction between them. We assume that orthonormal bases are obtained separately for the respective subsystems. A nonorthogonal basis $\{\varphi\}$ is formed by combining these bases, since eigenstates in different subsystems are in general not orthogonalized. Using the nonorthogonal basis, we address the eigenvalue problem

$$H|\psi_k\rangle = E_k|\psi_k\rangle, \quad (\text{B2})$$

where $\psi_k(E_k)$ is the k th eigenstate (eigenenergy). ψ_k is expanded in terms of the nonorthogonal basis as

$$|\psi_k\rangle = \sum_j |\varphi_j\rangle c_{jk}, \quad (\text{B3})$$

and substituted into Eq. (B2). Multiplying both sides by $\langle\varphi_i|$ from the left, we have

$$\sum_j [S_{ij}(\varepsilon_j - E_k) + V_{ij}]c_{jk} = 0, \quad (\text{B4})$$

with the j th eigenenergy ε_j of H_0 , overlap integral $S_{ij} \equiv \langle\varphi_i|\varphi_j\rangle$, and coupling matrix element $V_{ij} = \langle\varphi_i|V|\varphi_j\rangle$. Since the eigenstates in $\{\varphi\}$ are normalized but orthogonalized only in the respective subsystems, $S_{ij} = \delta_{ij}$ for φ_i and φ_j in the same subsystem, while $S_{i\neq j} \sim \mathcal{O}(V_{i\neq j})$ for those in different subsystems. The latter is justified by the MWH approximation [92,93]

$$V_{ij} \propto S_{ij} \frac{V_{ii} + V_{jj}}{2}. \quad (\text{B5})$$

In what follows, we treat V as a perturbation and develop a perturbation theory based on the nonorthogonal basis, considering $S_{i\neq j}$ to be of the first order of smallness in $V_{i\neq j}$.

2. Perturbation expansion

To solve Eq. (B4) perturbatively, eigenenergy E_k and coefficient c_{jk} are expanded as

$$E_k = E_k^{(0)} + E_k^{(1)} + \dots, \quad (\text{B6})$$

$$c_{jk} = c_{jk}^{(0)} + c_{jk}^{(1)} + \dots, \quad (\text{B7})$$

and substituted into Eq. (B4). Here and in what follows, superscript (n) stands for the n th order in V . From the zeroth- and first-order terms, we have

$$(\varepsilon_i - E_k^{(0)})c_{ik}^{(0)} = 0, \quad (\text{B8})$$

$$-\delta_{ik}E_k^{(1)} + V_{ik} + (\varepsilon_i - \varepsilon_k)c_{ik}^{(1)} = 0, \quad (\text{B9})$$

which take the same forms as those derived for an orthogonal basis. Clearly, Eq. (B8) is satisfied by setting

$$E_k^{(0)} = \varepsilon_k, \quad c_{ik}^{(0)} = \delta_{ik}. \quad (\text{B10})$$

To restrict ourselves to nondegenerate perturbation theory, we assume $\varepsilon_i \neq \varepsilon_k$ for different indices $i \neq k$ in Eq. (B9). In the adsorption system, this is satisfied if i and k are assigned to a state of the free adsorbate and that of the clean surface, respectively, which are in general nondegenerate. By setting $i = k$ and $i \neq k$ in Eq. (B9), we obtain the first-order corrections to the eigenenergy and the coefficient

$$E_k^{(1)} = V_{kk}, \quad (\text{B11})$$

$$c_{ik}^{(1)} = -\frac{V_{ik}}{\varepsilon_i - \varepsilon_k} \quad (i \neq k), \quad (\text{B12})$$

respectively. In addition, $c_{kk}^{(1)}$ is determined from the normalization condition of ψ_k as

$$1 = \langle \psi_k | \psi_k \rangle = 1 + 2\text{Re}[c_{kk}^{(1)}] + \mathcal{O}(V^2), \quad (\text{B13})$$

which results in $c_{kk}^{(1)} = 0$ by setting c_{kk} to be real [94].

From the second-order terms in (B4), we have

$$\begin{aligned} -S_{ik}V_{kk} - \delta_{ik}E_k^{(2)} + \sum_{j(\neq k)} [S_{ij}(\varepsilon_j - \varepsilon_k) + V_{ij}]c_{jk}^{(1)} \\ - V_{kk}c_{ik}^{(1)} + (\varepsilon_i - \varepsilon_k)c_{ik}^{(2)} = 0, \end{aligned} \quad (\text{B14})$$

where overlap integrals appear explicitly. In the same way as for Eq. (B9), we obtain second-order corrections

$$E_k^{(2)} = \sum_{j(\neq k)} \left[\frac{|V_{kj}|^2}{\varepsilon_k - \varepsilon_j} - S_{kj}V_{jk} \right], \quad (\text{B15})$$

$$\begin{aligned} c_{ik}^{(2)} = \sum_{j(\neq k)} \frac{V_{ij}V_{jk}}{(\varepsilon_i - \varepsilon_k)(\varepsilon_j - \varepsilon_k)} - \frac{V_{ik}V_{kk}}{(\varepsilon_i - \varepsilon_k)^2} \\ + \frac{1}{\varepsilon_i - \varepsilon_k} \sum_j S_{ij}V_{jk} \quad (i \neq k), \end{aligned} \quad (\text{B16})$$

$$c_{kk}^{(2)} = -\frac{1}{2} \sum_{j(\neq k)} \left[\frac{|V_{kj}|^2}{(\varepsilon_k - \varepsilon_j)^2} + \frac{2\text{Re}(S_{kj}V_{jk})}{\varepsilon_k - \varepsilon_j} \right]. \quad (\text{B17})$$

One can readily confirm that the conventional perturbation formulas for an orthonormal basis can be reproduced by setting $S_{ij} = \delta_{ij}$ in Eqs. (B15)–(B17).

3. Adsorption energy

To apply the perturbation formulas derived above to molecular adsorption, we assume that V acts only between the states of the adsorbate and those of the surface, i.e., $E_j^{(1)} = 0$ for all j . This means that, up to the second order in V , the energy correction to φ_k is given by Eq. (B15), which consists of interactions between φ_k and the remaining. In particular, the interaction energy with φ_l is given by

$$\Delta\varepsilon_{kl} \simeq \frac{|V_{kl}|^2}{\varepsilon_k - \varepsilon_l} - S_{kl}V_{lk}. \quad (\text{B18})$$

For simplicity, we assume that the adsorption has little influence on the occupations of the two states. If both φ_k and φ_l are occupied, the first term in Eq. (B18) is canceled out by the counterpart $\Delta\varepsilon_{lk}$, while the second term, which is approximated to be

$$-S_{kl}V_{lk} \simeq \alpha|S_{kl}|^2 \quad (\text{B19})$$

with $\alpha > 0$ [92,93], leads to destabilization. Conversely, a stable bonding state is realized when either of the two states is occupied; i.e., an occupied state of the adsorbate (surface) interacts with an unoccupied state of the surface (adsorbate), which can be considered as donation (back-donation) of electronic charge from the adsorbate (surface) to the surface (adsorbate). The contribution of hybridization to the adsorption energy is mainly described by the sum of Eq. (B18) over k and l with large $|V_{kl}|$ and $\varepsilon_k \lesssim \varepsilon_F \lesssim \varepsilon_l$ or $\varepsilon_l \lesssim \varepsilon_F \lesssim \varepsilon_k$.

4. Overlap population

We next consider the overlap of states between the adsorbate and the surface. To this end, we assume that the nonorthogonal basis set $\{\varphi\}$ is composed of two orthogonal subsets A and B formed separately for the free adsorbate and the clean surface, respectively, and rewrite Eq. (B3) as

$$|\psi_k\rangle = \sum_{i \in A} |\varphi_i\rangle c_{ik} + \sum_{j \in B} |\varphi_j\rangle c_{jk}. \quad (\text{B20})$$

Since $S_{ij} = \delta_{ij}$ for $i, j \in A$ or B , the normalization condition for ψ_k is given by

$$1 = \sum_{i \in A} |c_{ik}|^2 + 2 \sum_{i \in A} \sum_{j \in B} \text{Re}(c_{ik}^* S_{ij} c_{jk}) + \sum_{j \in B} |c_{jk}|^2, \quad (\text{B21})$$

in which $|c_{ik}|^2$ and $|c_{jk}|^2$ are the net populations related to ψ_k of φ_i of the adsorbate and φ_j of the surface, respectively, while

$$p_{ijk} = 2\text{Re}(c_{ik}^* S_{ij} c_{jk}) \quad (\text{B22})$$

is the overlap population between them [86–88]. It is convenient to introduce the density of states weighted by overlap population

$$\rho_{ij}(\varepsilon) = \sum_k p_{ijk} \delta(\varepsilon - \varepsilon_k), \quad (\text{B23})$$

which visualizes the distribution of the overlap population as a function of energy. The contributions of all the occupied states to the overlap population between φ_i and φ_j is obtained from a sum of p_{ijk} over k such that $\varepsilon_k < \varepsilon_F$, or equivalently from

an integral of $\rho_{ij}(\varepsilon)$ up to ε_F , as

$$p_{ij} = \sum_k^{\varepsilon_k < \varepsilon_F} p_{ijk} = \int_{-\infty}^{\varepsilon_F} \rho_{ij}(\varepsilon) d\varepsilon. \quad (\text{B24})$$

Moreover, the states of the surface are usually treated collectively by defining

$$\rho_i(\varepsilon) = \sum_{j \in B} \rho_{ij}(\varepsilon) = \sum_{j \in B} \sum_k p_{ijk} \delta(\varepsilon - \varepsilon_k), \quad (\text{B25})$$

which is COOP discussed in Sec. III D.

To treat overlap population perturbatively, expansion

$$p_{ijk} = p_{ijk}^{(0)} + p_{ijk}^{(1)} + p_{ijk}^{(2)} + \dots, \quad (\text{B26})$$

and the perturbation formulas derived above are substituted to Eq. (B22). The zeroth-, first-, and second-order terms read

$$p_{ijk}^{(0)} = p_{ijk}^{(1)} = 0, \quad (\text{B27})$$

$$p_{ijk}^{(2)} = \frac{2\text{Re}(S_{ij}V_{ji})}{\varepsilon_i - \varepsilon_j} (\delta_{ik} - \delta_{jk}). \quad (\text{B28})$$

Thus, up to the second order in V , we obtain approximate expressions for overlap population

$$p_{ijk} \simeq \frac{2\text{Re}(S_{ij}V_{ji})}{\varepsilon_i - \varepsilon_j} (\delta_{ik} - \delta_{jk}) \quad (\text{B29})$$

and weighted density of states

$$\rho_{ij}(\varepsilon) \simeq \frac{2\text{Re}(S_{ij}V_{ji})}{\varepsilon_i - \varepsilon_j} [\delta(\varepsilon - \varepsilon_i) - \delta(\varepsilon - \varepsilon_j)], \quad (\text{B30})$$

which enable a better understanding of these quantities. It is clear from Eq. (B29) that the contribution to p_{ij} derives only from the situation in which either φ_i or φ_j is occupied, as in the case of adsorption energy (see Appendix B 3). If $\varepsilon_i < \varepsilon_F < \varepsilon_j$, for example, the contributions of occupied states to overlap population add up to

$$p_{ij} \simeq \frac{2\text{Re}[S_{ij}V_{ji}]}{\varepsilon_i - \varepsilon_j}. \quad (\text{B31})$$

Correspondingly, Eq. (B30) indicates that $\rho_{ij}(\varepsilon)$ displays a positive (negative) peak at $\varepsilon = \varepsilon_i$ (ε_j), signaling the formation of a bonding (antibonding) state, although the peak actually observed should be shifted by $\simeq \Delta\varepsilon_{ij}$ ($\Delta\varepsilon_{ji}$).

-
- [1] J. Hou, Y. Shao, M. W. Ellis, R. B. Moore, and B. Yi, *Phys. Chem. Chem. Phys.* **13**, 15384 (2011).
- [2] X. Huang, X. Qi, F. Boey, and H. Zhang, *Chem. Soc. Rev.* **41**, 666 (2012).
- [3] S. H. Hur and J.-N. Park, *Asia-Pac. J. Chem. Eng.* **8**, 218 (2013).
- [4] S. Zhang, Y. Shao, G. Yin, and Y. Lin, *J. Mater. Chem. A* **1**, 4631 (2013).
- [5] J. Nakamura and T. Kondo, *Top. Catal.* **56**, 1560 (2013).
- [6] H. Huang and X. Wang, *J. Mater. Chem. A* **2**, 6266 (2014).
- [7] X. Zhou, J. Qiao, L. Yang, and J. Zhang, *Adv. Energy Mater.* **4**, 1301523 (2014).
- [8] N. M. Julkapli and S. Bagheri, *Int. J. Hydrogen Energ.* **40**, 948 (2015).
- [9] L. T. Soo, K. S. Loh, A. B. Mohamad, W. R. W. Daud, and W. Y. Wong, *Appl. Catal. A-Gen.* **497**, 198 (2015).
- [10] D. Higgins, P. Zamani, A. Yu, and Z. Chen, *Energy Environ. Sci.* **9**, 357 (2016).
- [11] S. Kang, H. Kim, and Y.-H. Chung, *Nano Convergence* **5**, 13 (2018).
- [12] E. Yoo, T. Okata, T. Akita, M. Kohyama, J. Nakamura, and I. Honma, *Nano Lett.* **9**, 2255 (2009).
- [13] Y. Shao, S. Zhang, C. Wang, Z. Nie, J. Liu, Y. Wang, and Y. Lin, *J. Power Sources* **195**, 4600 (2010).
- [14] E. Yoo, T. Okada, T. Akita, M. Kohyama, I. Honma, and J. Nakamura, *J. Power Sources* **196**, 110 (2011).
- [15] S. Sun, G. Zhang, N. Gauquelin, N. Chen, J. Zhou, S. Yang, W. Chen, X. Meng, D. Geng, M. N. Banis, R. Li, S. Ye, S. Knights, G. A. Botton, T.-K. Sham, and X. Sun, *Sci. Rep.* **3**, 1775 (2013).
- [16] K. Yamazaki, Y. Maehara, C.-C. Lee, J. Yoshinobu, T. Ozaki, and K. Gohara, *J. Phys. Chem. C* **122**, 27292 (2018).
- [17] N. Cheng, S. Stambula, D. Wang, M. N. Banis, J. Liu, A. Riese, B. Xiao, R. Li, T.-K. Sham, L.-M. Liu, G. A. Botton, and X. Sun, *Nat. Commun.* **7**, 13638 (2016).
- [18] K.-J. Kong, Y. Choi, B.-H. Ryu, J.-O. Lee, and H. Chang, *Mater. Sci. Eng. C* **26**, 1207 (2006).
- [19] Y. Okamoto, *Chem. Phys. Lett.* **420**, 382 (2006).
- [20] D. H. Chi, N. T. Cuong, N. A. Tuan, Y.-T. Kim, H. T. Bao, T. Mitani, T. Ozaki, and H. Nagao, *Chem. Phys. Lett.* **432**, 213 (2006).
- [21] N. T. Cuong, A. Fujiwara, T. Mitani, and D. H. Chi, *Comput. Mater. Sci.* **44**, 163 (2008).
- [22] K. Okazaki-Maeda, Y. Morikawa, S. Tanaka, and M. Kohyama, *Surf. Sci.* **604**, 144 (2010).
- [23] M. Zhou, A. Zhang, Z. Dai, Y. P. Feng, and C. Zhang, *J. Phys. Chem. C* **114**, 16541 (2010).
- [24] D. Xian-Qi, T. Ya-Nan, D. Ya-Wei, L. Yan-Hui, Z. Jian-Hua, Z. Bao, and Y. Zong-Xian, *Chin. Phys. B* **20**, 056801 (2011).
- [25] Y. Tang, Z. Yang, and X. Dai, *J. Chem. Phys.* **135**, 224704 (2011).
- [26] I. Fampiou and A. Ramasubramaniam, *J. Phys. Chem. C* **116**, 6543 (2012).
- [27] T. Yumura, T. Awano, H. Kobayashi, and T. Yamabe, *Molecules* **17**, 7941 (2012).
- [28] G. Ramos-Sanchez and P. B. Balbuena, *Phys. Chem. Chem. Phys.* **15**, 11950 (2013).
- [29] T.-u. Park, Y. Tomita, and T. Nakayama, *Surf. Sci.* **621**, 7 (2014).
- [30] A. Chutia, I. Hamada, and M. Tokuyama, *Surf. Sci.* **628**, 116 (2014).
- [31] F. Ferrante, A. Prestianni, R. Cortese, R. Schimmenti, and D. Duca, *J. Phys. Chem. C* **120**, 12022 (2016).
- [32] L. G. Verga, J. Aarons, M. Sarwar, D. Thompsett, A. E. Russell, and C.-K. Skylaris, *Phys. Chem. Chem. Phys.* **18**, 32713 (2016).
- [33] R. N. Lenz Baldez, P. Piquini, A. A. Schmidt, and M. A. Kuroda, *Phys. Chem. Chem. Phys.* **19**, 22153 (2017).
- [34] S. A. Wella, Y. Hamamoto, Suprijadi, Y. Morikawa, and I. Hamada, *Nanoscale Adv.* **1**, 1165 (2019).

- [35] A. V. Krashennnikov, P. O. Lehtinen, A. S. Foster, P. Pyykkö, and R. M. Nieminen, *Phys. Rev. Lett.* **102**, 126807 (2009).
- [36] O. Üzengi Aktürk and M. Tomak, *Phys. Rev. B* **80**, 085417 (2009).
- [37] X.-Q. Dai, Y.-N. Tang, J.-H. Zhao, and Y.-W. Dai, *J. Phys.: Condens. Matter* **22**, 316005 (2010).
- [38] P. Błoński and J. Hafner, *J. Chem. Phys.* **134**, 154705 (2011).
- [39] Y. Tang, Z. Yang, and X. Dai, *J. Magn. Magn. Mater.* **323**, 2441 (2011).
- [40] D. Xu, J. Zhao, and X. Wang, *J. Nanopart. Res.* **15**, 1590 (2013).
- [41] Y. Tang, Y. Tang, Z. Yang, Z. Yang, X. Dai, and X. Dai, *J. Nanosci. Nanotechnol.* **13**, 1612 (2013).
- [42] Q. Qi, H. Liu, W. Feng, H. Tian, H. Xu, and X. Huang, *Comput. Mater. Sci.* **96**, 268 (2015).
- [43] H. Shi, S. M. Auerbach, and A. Ramasubramaniam, *J. Phys. Chem. C* **120**, 11899 (2016).
- [44] C. R. C. Rêgo, P. Tereshchuk, L. N. Oliveira, and J. L. F. Da Silva, *Phys. Rev. B* **95**, 235422 (2017).
- [45] C. K. Acharya, D. I. Sullivan, and C. H. Turner, *J. Phys. Chem. C* **112**, 13607 (2008).
- [46] J. Wu, S. W. Ong, H. C. Kang, and E. S. Tok, *J. Phys. Chem. C* **114**, 21252 (2010).
- [47] G. Kim and S.-H. Jhi, *ACS Nano* **5**, 805 (2011).
- [48] D.-H. Lim and J. Wilcox, *J. Phys. Chem. C* **115**, 22742 (2011).
- [49] D. Xu, Y. Tian, J. Zhao, and X. Wang, *J. Nanopart. Res.* **17**, 25 (2015).
- [50] L. G. Verga, A. E. Russell, and C.-K. Skylaris, *Phys. Chem. Chem. Phys.* **20**, 25918 (2018).
- [51] Y. Tang, Z. Yang, and X. Dai, *J. Nanopart. Res.* **14**, 844 (2012).
- [52] I. Fampiou and A. Ramasubramaniam, *J. Phys. Chem. C* **117**, 19927 (2013).
- [53] G. Ramos-Sánchez and P. Balbuena, *J. Electroanal. Chem.* **716**, 23 (2014).
- [54] M. Mahmoodinia, P.-O. Åstrand, and D. Chen, *J. Phys. Chem. C* **121**, 20802 (2017).
- [55] M. Zhou, A. Zhang, Z. Dai, C. Zhang, and Y. P. Feng, *J. Chem. Phys.* **132**, 194704 (2010).
- [56] Y. Tang, Z. Yang, and X. Dai, *Phys. Chem. Chem. Phys.* **14**, 16566 (2012).
- [57] G. Kim, Y. Kawazoe, and K.-R. Lee, *J. Phys. Chem. Lett.* **3**, 1989 (2012).
- [58] Y. Tang, Z. Lu, W. Chen, W. Li, and X. Dai, *Phys. Chem. Chem. Phys.* **17**, 11598 (2015).
- [59] I. Fampiou and A. Ramasubramaniam, *J. Phys. Chem. C* **119**, 8703 (2015).
- [60] C. S. Wang, H. Wang, R. Wu, and R. Ragan, *J. Phys. Chem. C* **122**, 21919 (2018).
- [61] W. Qin and X. Li, *J. Phys. Chem. C* **114**, 19009 (2010).
- [62] R. J. Gasper and A. Ramasubramaniam, *J. Phys. Chem. C* **120**, 17408 (2016).
- [63] D.-H. Lim and J. Wilcox, *J. Phys. Chem. C* **116**, 3653 (2012).
- [64] Y. Tian, Y.-j. Liu, J.-x. Zhao, and Y.-h. Ding, *RSC Adv.* **5**, 34070 (2015).
- [65] H.-H. Liu, K.-L. Hsueh, and C.-W. Hong, *Electrochim. Acta* **259**, 598 (2018).
- [66] S. Back, J. Lim, N.-Y. Kim, Y.-H. Kim, and Y. Jung, *Chem. Sci.* **8**, 1090 (2017).
- [67] B. Hammer, O. Nilsen, and J. K. Nørskov, *Catal. Lett.* **46**, 31 (1997).
- [68] S. A. Wella, Y. Hamamoto, F. Iskandar, Suprijadi, Y. Morikawa, and I. Hamada, *J. Chem. Phys.* **152**, 104707 (2020).
- [69] N. Troullier and J. L. Martins, *Phys. Rev. B* **43**, 1993 (1991).
- [70] J. P. Perdew, K. Burke, and M. Ernzerhof, *Phys. Rev. Lett.* **77**, 3865 (1996).
- [71] M. Otani and O. Sugino, *Phys. Rev. B* **73**, 115407 (2006).
- [72] I. Hamada, M. Otani, O. Sugino, and Y. Morikawa, *Phys. Rev. B* **80**, 165411 (2009).
- [73] R. H. Telling, C. P. Ewels, A. A. El-Barbary, and M. I. Heggie, *Nat. Mater.* **2**, 333 (2003).
- [74] A. A. El-Barbary, R. H. Telling, C. P. Ewels, M. I. Heggie, and P. R. Briddon, *Phys. Rev. B* **68**, 144107 (2003).
- [75] S. Malola, H. Häkkinen, and P. Koskinen, *Appl. Phys. Lett.* **94**, 043106 (2009).
- [76] X. Q. Dai, J. H. Zhao, M. H. Xie, Y. N. Tang, Y. H. Li, and B. Zhao, *Eur. Phys. J. B* **80**, 343 (2011).
- [77] S. T. Skowron, I. V. Lebedeva, A. M. Popov, and E. Bichoutskaia, *Chem. Soc. Rev.* **44**, 3143 (2015).
- [78] G. Hennig, *J. Appl. Phys.* **36**, 1482 (1965).
- [79] R. Henson and W. Reynolds, *Carbon* **3**, 277 (1965).
- [80] Y. Ma, P. O. Lehtinen, A. S. Foster, and R. M. Nieminen, *New J. Phys.* **6**, 68 (2004).
- [81] C. Dong, W. Zhu, S. Zhao, P. Wang, H. Wang, and W. Yang, *J. Appl. Mech.* **80**, 040904 (2013).
- [82] E. Kano, A. Hashimoto, and M. Takeguchi, *Appl. Phys. Express* **10**, 025104 (2017).
- [83] B. Hammer and J. K. Nørskov, *Nature (London)* **376**, 238 (1995).
- [84] B. Hammer and J. K. Nørskov, *Surf. Sci.* **343**, 211 (1995).
- [85] B. Hammer, Y. Morikawa, and J. K. Nørskov, *Phys. Rev. Lett.* **76**, 2141 (1996).
- [86] R. McWeeny, *J. Chem. Phys.* **19**, 1614 (1951).
- [87] R. S. Mulliken, *J. Chem. Phys.* **23**, 1833 (1955).
- [88] R. S. Mulliken, *J. Chem. Phys.* **23**, 1841 (1955).
- [89] R. Hoffmann, *Rev. Mod. Phys.* **60**, 601 (1988).
- [90] H. Aizawa and S. Tsuneyuki, *Surf. Sci.* **399**, L364 (1998).
- [91] G. Blyholder, *J. Phys. Chem.* **68**, 2772 (1964).
- [92] R. S. Mulliken, *J. Phys. Chem.* **56**, 295 (1952).
- [93] M. Wolfsberg and L. Helmholz, *J. Chem. Phys.* **20**, 837 (1952).
- [94] See, e.g., W. Greiner, *Quantum Mechanics: An Introduction*, 4th ed. (Springer, New York, 2001).